

Desorption Dynamics, Internal Energies and Imaging of Organic Molecules from Surfaces with Laser Desorption and Vacuum Ultraviolet (VUV) Photoionization

Oleg Kostko,^[a] Lynelle K. Takahashi,^[a,b] and Musahid Ahmed*^[a]

^[a]Chemical Sciences Division, Lawrence Berkeley National Laboratory, Berkeley, CA 94720

^[b]Department of Chemistry, University of California at Berkeley, Berkeley, CA 94720

Abstract: There is enormous interest in visualizing the chemical composition of organic material that comprises our world. A convenient method to obtain molecular information with high spatial resolution is imaging mass spectrometry. However, the internal energy deposited within molecules upon transfer to the gas phase from a surface can lead to increased fragmentation and to complications in analysis of mass spectra. Here it is shown that in laser desorption with postionization by tunable vacuum ultraviolet (VUV) radiation, the internal energy gained during laser desorption leads to minimal fragmentation of DNA bases. The internal temperature of laser-desorbed triacontane molecules approaches 670 K, whereas the internal temperature of thymine is 800 K. A synchrotron-based VUV postionization technique for determining translational temperatures reveals that biomolecules have translational temperatures in the range of 216-346 K. The observed low translational temperatures, as well as their decrease with increased desorption laser power is explained by collisional cooling. An example of imaging mass spectrometry on an organic polymer, using laser desorption VUV postionization shows 5 μm feature details while using a 30 μm laser spot size and 7 ns duration. Applications of laser desorption postionization to the analysis of cellulose, lignin and humic acids are briefly discussed.

Keywords: synchrotron VUV, desorption dynamics, nucleic acids, imaging mass spectrometry, scanning probe microscopy

Introduction

Imaging the chemical composition of material that comprises our world is of great interest in understanding and preserving it. Developing new microscopies to detect and identify organic molecules with high spatial resolution will afford the necessary molecular specificity to probe

complex nano-scale chemistry. For instance, visualizing the organic composition of atmospheric aerosol particle surfaces can promote understanding of the critical roles aerosols play in global climate change^[1] and on the radiative balance and chemistry of the troposphere. Biological molecules are critical determinants in the structure and dynamics at boundaries of different cellular structures.^[2] These molecules play important roles in the regulation of both intra- and inter-cellular processes, including metabolic activity, protein synthesis, host–pathogen interactions and cell motility. Many of these cellular processes involve reactions over different spatial locations or chemical gradients, for example, within a lipid bilayer.^[3] The development of chemically sensitive methods to image the distribution of small molecules in cells would provide a key experimental tool.

Biological systems are now being viewed both as possible sources of alternative energy and environmental bio-remediation. For instance, plant based lignocellulosic material are being seen as potential biofuels,^[4] while different bacteria are being considered for environmental bio-remediation.^[5] Interestingly, similar types of molecules that are present on the surfaces of different biological systems, such as fatty acids, long chain linear and branched hydrocarbons, and a variety of oxidized hydrocarbon species,^[6, 7] are also thought to be present on the surfaces of tropospheric aerosols.^[8-10] Furthermore, similar molecules are thought to be prevalent in soil organic matter^[11, 12] and it would be beneficial to have access to a set of tools which will allow visualization of these molecules. Towards this end, laser desorption mass spectrometry coupled to synchrotron vacuum ultraviolet (VUV) postionization is being developed. Single photon ionization (SPI) with VUV radiation, when combined with high spatial resolution, could offer unprecedented chemical specificity for mass spectral imaging of organic structures and surfaces.

In an effort to understand VUV photoionization of the kinds of molecules expected to be important in biological systems, aerosols, and soil organic matter, a number of test molecules, ranging from DNA bases, soil extracts (humic acids), plant biopolymers, and long-chain hydrocarbons, were selected for study. To fully exploit the chemical specificity of SPI for mass spectral imaging, the fragmentation of the parent cation must be minimized. Preserving parent molecular ions in a mass spectrum is essential for generating chemically detailed maps of complex samples. It is well-known that the amount of fragmentation in a mass spectrum is extremely sensitive to the amount of internal energy within the parent ion or neutral

molecule.^[13, 14] Clearly, threshold ionization reduces the amount of fragmentation in a mass spectrum by minimizing the internal excitation of the molecules during the ionization step.^[15]

For large molecules (long-chain hydrocarbons or biomolecules), the internal energy imparted to the neutral molecule in order to introduce it into the gas phase is equally as important as the energy imparted upon photoionization. In order to preserve the fragile molecular ion, supersonic jet cooling of the internal degrees of freedom is usually required.^[16, 17] Since supersonic jet cooling cannot be easily incorporated into surface imaging experiments, the internal energy of the ion or laser desorbed neutrals could pose a significant problem in imaging mass spectrometry. To evaluate this potential obstacle, experiments were conducted by combining laser desorption with VUV postionization. These experiments will show that the neutral molecule can be detected via its parent molecular ion with high signal-to-noise-ratios and that the degree of fragmentation can be finely controlled or, in some cases, eliminated entirely.

Early reviews of attempts to quantify energies imparted into molecules formed in laser desorption are provided by Levis and Hanley.^[18, 19] Molecular-level understanding of desorption processes, particularly as applied to MALDI, using molecular dynamics simulations and experiments have been attempted by Knochenmuss, Zhigilei, Garrison and co-workers.^[20-22] Desorption dynamics have also been examined using a number of different techniques, particularly with relevance to organic aerosols, where the ionization step is separated from the desorption step of the experiment.^[23-26] Very recently, the internal energy of tryptophan and thymine formed upon ion-sputtering was quantified, and similar methods will be used here to ascertain internal energies from laser desorption.^[14]

Results and Discussion

Internal energy

Previous VUV secondary neutral mass spectrometry (VUV-SNMS) experiments have revealed that neutral biomolecules released from a surface after sputtering by 25 keV Bi_3^+ ions have about 2.5 eV of internal energy.^[14] While such high-energy ion beams are well-suited for high spatial resolution imaging down to 100 nm, this energy can yield significant amounts of molecular fragmentation. In this study, the energies imparted into neutral molecules desorbed

by a 349 nm laser are investigated using two different methods: one by utilizing fragmentation ratios and the second by measuring appearance energies of fragments.

Internal energy from fragmentation ratios. For the measurement of internal energy of hydrocarbons, the unbranched, long-chain hydrocarbon triacontane ($C_{30}H_{62}$) was chosen. Previously it was observed that the level of fragmentation of the parent molecule from pure triacontane aerosols strongly depends on the temperature at which the aerosols were flash vaporized.^[15] The dependence of the parent molecule fractional population on temperature with 10.7 eV photoionization was also determined (see Figure 2 in reference 15). Using this dependence, triacontane could be used as a molecular thermometer by observing the ratio of the parent and fragments and fitting the obtained fractional population into the calibration curve.

Due to the very different experimental conditions used in reference 15 and in this work (evaporation of aerosols vs. desorption from a bulk surface), the applicability of the aerosol curve relating parent molecule fractional population to molecular temperature was verified. A few milligrams of triacontane were placed on a heating/cooling stage inside of the experimental apparatus and heated to 333, 353 and 373 K. The mass spectrum, recorded for triacontane evaporated at 373 K and postionized with 10.5 eV synchrotron VUV radiation, is shown in Figure 1(a). The mass spectrum has a strong peak at $m/z=422$, corresponding to the triacontane parent, and a number of peaks with lower m/z , the intensities of which are much smaller than the intensity of the parent peak. The elevated baseline following the parent peak is due to the continuous postionization of evaporating triacontane by the quasi-continuous synchrotron VUV radiation.

For an evaporation temperature of 373 K, the parent constitutes 73% of the total signal and the fragments make up 27%. The good correlation of these values, as well as those at 333 and 353 K, with the values obtained from the aerosol experiment is shown in Figure 2. This assures the applicability of the temperature dependence of the triacontane fractional population obtained in reference 15 to the current experiment.

The mass spectrum obtained for laser-desorbed triacontane is shown in Figure 1(b). For the collection of the mass spectrum, a 5 μs extraction pulse was applied to the ion optics 1 μs after the desorption laser pulse. 10.5 eV synchrotron VUV radiation was used for postionization. In this case, most of the triacontane parent is fragmented, and the mass spectrum exhibits a

fragmentation pattern dominated by sequential elimination of CH₂. The fractional populations in this case are 0.09 for the parent molecule and 0.91 for the fragments. These values are fit to the fractional population dependence curve shown in Figure 2. The temperature corresponding to the observed laser-ablated triacontane fractional population corresponds to an internal temperature of 670 K.

In order to determine the corresponding energy for an internal temperature of 670 K, the average vibrational energy of triacontane is approximated by a collection of harmonic oscillators:^[13, 14]

$$E_{vib} = \sum_{i=1}^s \frac{h\nu_i}{e^{(h\nu_i/kT)} - 1}. \quad (1)$$

The molecular structure of triacontane was optimized and the vibrational frequencies were computed using Gaussian 03^[27] structure calculation software at the B3LYP/6-311G level of theory. Using this approximation, it was found that the temperature of 670 K corresponds to an internal energy of 4.6 eV. This value of internal energy arises due to the large number of vibrational modes for triacontane (270 vs. 39 vibrational modes for thymine).

Internal energy from appearance energies of fragments. For laser-desorbed thymine (C₅H₆N₂O₂), a different approach was used to measure the internal energy. In this approach, the energy tunability of the synchrotron VUV source was utilized to collect mass spectra at various photon energies. The signal intensities from the molecular parent (m/z = 126) and the main fragment of thymine (m/z = 83) are then plotted versus photon energy to produce their photoionization efficiency (PIE) curves. PIE curves of the parent and fragment of thymine are shown in Figure 3.

The first set of data in Figure 3, shown by a black solid line, corresponds to PIE curves of low-internal energy thymine molecules generated in a molecular beam.^[28, 29] Briefly, thymine was heated to 490 K and expanded together with argon (backing pressure of 34.7 kPa) through a 100 μm nozzle into vacuum, which led to adiabatic cooling of the thymine molecules. The experimental conditions in the molecular beam experiment were roughly comparable to the conditions used by Amirav et al., who observed a vibrational temperature below 50 K for molecules with similar weight.^[30] The onset of the PIE curve of the thymine parent (Figure 3(a)),

corresponds to an adiabatic ionization energy of 8.95 ± 0.05 eV,^[31] which correlates well with previous mass analyzed threshold ionization^[32] (8.9178 ± 0.0010 eV) and VUV-SPI (8.87 ± 0.05 eV^[33] and 8.82 ± 0.03 eV^[34]) experiments. Two signal spikes, observed in the region from 11.6 eV to 11.9 eV are due to two absorption transitions of argon used in the gas filter (at 11.62 and 11.83 eV). A correction of signal intensity using measured VUV photon fluence leads to the appearance of the observed discontinuity.

The thymine fragment C_4H_5NO ($m/z=83$) appears in the mass spectrum upon loss of HNCO (isocyanic acid). Its appearance energy is 10.95 ± 0.05 eV (see Figure 3(b)).

In order to obtain PIE curves of thymine which have more defined temperature conditions, the thymine film sample was placed on a heating/cooling stage and heated to 313 K inside the imaging apparatus. PIE curves obtained in this case using VUV ionization are shown in Fig. 3 by filled black circles. A good correlation of the PIE curves of thermally evaporated thymine to those from the molecular beam is immediately observed, demonstrating the small effect that the temperature increase to 313 K has on the PIE curves.

Laser desorption PIE curves for thymine and its fragment $m/z=83$ are shown in Figure 3 by open squares. The ion extraction pulse was applied 2 μ s after the laser desorption pulse. Desorbed neutral thymine molecules were postionized with tunable VUV radiation. The PIE curve for the parent is very similar to PIE curves for molecular beam and thermally evaporated thymine in the energy range between 8.0–10.6 eV. Above 10.6 eV, the PIE curve for laser desorbed thymine starts to deviate from the thermally evaporated thymine's PIE curve. It has been observed previously that the increase of internal energy of different molecules has very low if any influence on the ionization energy of the parent molecule.^[13, 35, 36] Such negligible thermal effects on the ionization energy have also been observed for thymine.^[14]

The ion signal curve for the laser-desorbed thymine fragment $m/z=83$ differs from those observed in the thermal evaporation and molecular beam experiments. The onset of the signal for laser desorption is around 10.2 eV, and is different from the 11.05 eV of thermally evaporated molecules and 10.95 eV for molecules in the molecular beam. The curves have similar shapes but in the case of laser desorption, the onset is red-shifted by 0.85 eV. This shift correlates well with the PIE curve shape observed for the parent starting from 10.6 eV and is due to the fragmentation of the parent ions into $m/z=83$ mass channel.

While the increase of internal energy has a negligible effect on the ionization energies, it leads to noticeable change in the fragment's appearance energy.^[35-37] It has been shown that the thermal (internal) energies, stored in the molecule and the energy added by photons, are equivalent in regard to dissociative photoionization.^[37] This would suggest that the increase of temperature of the parent molecule will eventually lead to a shift of the appearance energy of the molecular fragment by the value equal to the change in internal energy.

To determine the internal energy that corresponds to a shift of 0.85 eV in the appearance energy relative to thermally evaporated appearance energy, an approximation shown in equation (1) is used. The vibrational frequencies of thymine were computed using B3LYP/6-311+G(d, p) level of theory using optimized molecular structures obtained with same level of theory. The internal energy of thymine thermally evaporated at 313 K according to (1) is 0.15 eV. Similarly, the internal energy of laser-desorbed thymine is 1.00 eV, which corresponds to an internal temperature of 800 K. One should note here that the temperature of 800 K is a lower limit of the internal temperature, corresponding to the case when 100% of vibrational excitation goes into the dissociation of thymine molecules. When this process is less effective, higher internal energy is required to explain the observed shift in the experimental PIE curve.

Desorption dynamics and translational temperature

The translational temperatures of laser-desorbed neutral molecules were also measured to provide a better understanding of the desorption dynamics. In Figure 4, time of flight (TOF) distributions measured for adenine ($C_5H_5N_5$), thymine ($C_5H_6N_2O_2$), cytosine ($C_4H_5N_3O$) and uracil ($C_4H_4N_2O_2$) are shown. All four distributions have a similar shape, but different starting times, varying from $\sim 44 \mu s$ for cytosine to $\sim 50 \mu s$ for adenine. These differences in starting times correlate well with the different masses of the molecules. Adenine has a mass of 135 Da, thymine – 126 Da, cytosine – 111 Da and uracil – 112 Da.

For analysis of the TOF distributions, a half-space Maxwell-Boltzmann distribution was used. In order to directly fit the obtained experimental TOF curves, the Maxwell-Boltzmann distribution was modified to account for the TOF conditions:

$$I(t) \sim \left(\frac{L}{t-t_0} \right)^4 \exp \left[-\frac{m}{2kT} \left(\frac{L}{t-t_0} \right)^2 \right] + \text{baseline}. \quad (2)$$

Here L is a distance between the surface and ionizing VUV beam, m is the mass of the molecule, k is Boltzmann's constant, T is the molecular plume translational temperature, t corresponds to time of flight and t_0 appears in the equation because the start point of the TOF distribution is shifted during the flight in a TOF-mass spectrometer and is not equal to $0 \mu\text{s}$. A baseline term appears in the equation to account for background signal and for the broad peaks produced by molecular fragments that overlap with the analyzed parent peak.

The fitted curves, obtained for the experimental data used eq. (2) are shown in Figure 4. The excellent fit of the measured spectra with the idealized Maxwell-Boltzmann distribution suggests that the molecules in the desorbed molecular plume have well-defined translational temperature. The temperatures obtained from the fits are: 216 K for adenine, 329 K for thymine, 346 K for cytosine and 298 K for uracil. Using these temperatures, one can derive the mean and most probable translational velocities. The values of the velocities for the molecules investigated in this work are shown in Table 1, together with their translational energy values. It is immediately apparent that the translational energies are quite low and are in range of few tens of meV. The mean translational velocities for all four bases are comparable and for three of them lie in range of 235-257 m/s and only adenine has a lower velocity of 184 m/s.

Comparably low velocities were observed previously for laser-desorbed biomolecules. Spengler et al. found out that the translational temperature for tryptophan ($m/z = 204$) in their experiment was about 300 K,^[38] which corresponds to a mean velocity of 176 m/s. Tsai et al. demonstrated that in their experiment the velocity distributions of tryptophan and 2,4,6-trihydroxyacetophenone (THAP) cannot be fitted by a single Maxwell-Boltzmann distribution.^[39] Instead, they used three Maxwell-Boltzmann distributions to fit the experimental curve. The most probable velocities for these distributions were 61, 154 and 287 m/s for tryptophan and 127, 258 and 503 m/s for THAP. In the investigation of laser ablation of tryptophan-glycine (Trp-Gly), Elam and Levy observed a variety of average translational velocities and temperatures, depending on the experimental conditions. They noticed that the average velocity was in a range of 440 to 570 m/s for Trp-Gly film with addition of 0.1% of R6G laser dye. For the neat Trp-

Gly films the average velocities were found to be larger, in the range of 670 to 820 m/s.^[40] Engelke et al. determined the velocity distribution of phenylthiohydantoin-glycine ($m/z=192$), which has a mean translational velocity of 177 ± 7 m/s.^[41] Huth-Fehre and Becker measured the velocity distributions of neutral gramicidin S ($m/z=1141$) and ferulic acid ($m/z=194$), the latter of which was used as a matrix in their study.^[42] They observed almost identical velocity distributions for both of these substances, despite their very different masses, with the maximum of the distribution peaking between 300 and 400 m/s.

As is apparent from these previous works, there is no dependence observed in the translational velocities of different desorbed molecules on their mass. The translational velocities found in previous investigations and in the present study lie in range of several hundred meters per second, and as shown in ref.^[40] and discussed below, they depend considerably on the experimental conditions.

Collisional cooling in laser desorption

To understand the effect of desorption laser power on the translational temperature of molecules, the TOF distributions were measured for adenine coatings at four different laser peak power densities. The two resulting TOF spectra are shown in Figure 5 (a,b). The laser peak power densities used in these measurements are 451 MW/cm^2 for Fig. 5(a) and 194 MW/cm^2 for Fig. 5(b). The fit of the obtained TOF distributions with the Maxwell-Boltzmann distribution, eq. (2), revealed translational temperatures of 140 K and 208 K for high and low laser peak power densities, respectively. The translational temperatures of adenine molecules at four different desorption laser peak power densities are shown in Figure 5(c). The dependence is obtained for two sets of data and is shown together with the standard deviation of the measurements. A roughly linear decrease of translational temperature with an increase of desorption laser peak power density is observed. This counterintuitive behavior, when the lower translational temperature corresponds to higher desorption laser power, could be explained by the collisional cooling in the laser-desorbed molecular plume, when the stronger laser pulse desorbs a larger number of molecules, which subsequently leads to a larger number of intermolecular collisions.

Previously in molecular beam experiments, it was found that increasing the pressure of the gas which will expand leads to an increase in the number of collisions between the gas atoms or molecules and improved cooling of translational, vibrational and rotational degrees of

freedom.^[18, 43, 44] Since a similar cooling effect may be occurring during laser desorption, it is instructive to estimate the number of adenine molecules desorbed by a single laser shot from the sample surface and compare it to a model molecular beam experiment during a time interval typical for laser desorption.

To estimate the number of laser desorbed molecules one can use the following equation:

$$N = \frac{\rho V}{M} N_A, \quad (3)$$

where N is the number of molecules of the substance, which has volume V , density ρ and molar mass M . N_A corresponds to the Avogadro constant. To find the volume of adenine, which is desorbed by a single laser pulse, a combination of optical and atomic force microscopies and optical surface profilometry was used. During sample preparation it was discovered that adenine did not form a homogeneous layer within the samples, but tended to coalesce into microcrystals with size of several microns. The volume of the crystals and the density with which they cover the sample surface was estimated using the techniques mentioned above. These techniques revealed that the average height of the adenine microcrystals was $0.9 \mu\text{m}$ and that only about 30% of the sample surface was covered by adenine crystals. The size of the laser spot was determined using optical microscopy to have a diameter of $30 \mu\text{m}$. From this, the number of adenine molecules which can be desorbed from the sample surface by a $30 \mu\text{m}$ laser spot size was determined to be $1.36 \cdot 10^{12}$ molecules. The desorbed molecule signal decay time profile suggests that approximately ten laser shots were required to desorb all adenine from the sample surface. Hence $1.36 \cdot 10^{11}$ adenine molecules were desorbed per laser shot.

To model the laser desorption experiment as a molecular beam, the following approximation can be used. For a perfect gas (the conditions inside of the gas container with a nozzle can be approximated as a perfect gas) the equation of state is:

$$p = \frac{N}{V} kT, \quad (4)$$

where p is a pressure of the gas, N is number of molecules of the gas, V is the volume, T is the temperature, and k is Boltzmann's constant. Using equation (4) the number of molecules N can be estimated. Ambient conditions will be used for the pressure and temperature of the gas (101 kPa and 300 K, respectively). To find the volume of the gas V , the nozzle is approximated as a

cylinder. In this case, the diameter of the cylinder (nozzle) corresponds to the 30 μm diameter of the laser desorption crater. The height of the cylinder equals the product of gas velocity and time. A desorption laser pulse width of 7 ns is used in this calculation. The most probable speed ($v_{\text{prob}}=(2kT/m)^{1/2}$), obtained from the Maxwell-Boltzmann distribution for room temperature adenine gas is used as the velocity and is 192 m/s. This calculation estimates $2.3 \cdot 10^{10}$ adenine molecules escaping through a 30 μm nozzle during 7 ns.

These two rough estimations give approximately the same order of magnitude for the number of molecules escaping from either the surface of a sample or through a nozzle during a similar time. Thus collisional cooling, widely observed in molecular beams, should play a significant role in the case of laser desorption as well. This cooling leads to a decrease of the translational temperature and should subsequently lead to a reduction of internal energy.

Previously it was observed that increasing the laser fluence led to an increase in the number of desorbed species, and this agrees well with the collisional cooling in the laser desorption plume proposed above. Poretzky et al. and Ermer et al. observed an increase of ion desorption yield of two MALDI matrices, 3-hydroxypicolinic and 2,5-dihydroxybenzoic acids, correspondingly, with increase of laser fluence.^[45, 46] Krajnovich in his investigation of laser sputtering of highly oriented pyrolytic graphite^[47] has observed an increase of flux of desorbed neutral atomic carbon and carbon dimers and trimers with increasing laser fluence. He also observed that the mean translational energy of these species grew with an increase in laser fluence. Similar behavior of translational energy was observed by Georgiou et al. for ablation of chlorobenzene films.^[48] On the contrary, Grivas et al. stated that the Knudsen layer temperature (translational temperature in the vicinity of the surface area of the laser irradiated material) of polyarylsulfone films decreased with increasing laser fluence.^[49] They explained this behavior as we do here, that increasing number of collisions among the desorption products, when fluence is increased, led to enhanced collisional cooling.

Imaging Mass Spectrometry

The ultimate aim of these dynamics and energy studies is to provide a knowledge base and an experimental platform to perform imaging mass spectrometry using laser desorption with VUV postionization of fragile organic molecules. Towards this end, a surface scan of a test sample was undertaken. The optical microscope image of the sample surface is shown in Figure

6 (a). The sample is a silicon wafer covered with a photoresist polymer etched with features of different sizes. The sample field of view shown in Figure 6(a) is 700 μm x 700 μm , and the smallest features are 5 μm in size. The mass spectrum of the laser-desorbed photoresist with photoionization with 10.5 eV synchrotron radiation is shown in Figure 7(a). The spatial distribution of a peak of average intensity in the mass spectrum ($m/z=165$) is shown in Figure 6(b). For the scan, 256 laser shots per surface spot and 5 μm step sizes between spots were used. The laser power was chosen such that no silicon ablation was observed. For the detection of Si signal in the mass spectrum, significantly higher laser intensity is required.

Comparison of the optical microscope image of the sample (Fig. 6(a)) with the laser desorption image (Fig. 6(b)) shows very good agreement and reproducibility of even the smallest features. Optical microscopy revealed that the size of the laser desorption spots over the polymer is about 10 μm . This can also be observed in cross-sections A and B (shown in Figure 6(b)) of the laser desorption image, intensity profiles of which are shown in Figure 7 (b,c). For comparison, idealized profiles of the photoresist on the surface of the silicon wafer are also shown in Figure 7(b,c). In Fig. 7(b) one may see that the experimental profiles have approximately a Gaussian shape. To test the size of the laser beam, the profile of an ideal feature (shown by black solid line in Figure 7(b)) was convoluted by a Gaussian with 10 μm full width at half maximum. The resulting curve (dashed line in Fig 7(b)) demonstrates perfect agreement with the experimental data and proves that the laser desorption spot size in this experiment reaches 10 μm .

This may be surprising since a 30 μm laser spot size, observed for biomolecules, is reduced to 10 μm over the polymer film. This is due to the Gaussian spatial profile of the laser irradiation intensity, which leads to the following dependence of the squared spot diameter D^2 on the maximum laser pulse peak power P_0 :^[50, 51]

$$D^2 = 2w^2 \ln\left(\frac{P_0}{P_{th}}\right), \quad (5)$$

where w is the actual beam radius and P_{th} is the threshold fluence for the material. Figure 7(d) shows a linear dependence of the experimental squared spot diameter on the laser peak power in a semilog plot and could be fit with eq. (5). This means that choice of low laser powers will lead to an decrease of laser spot size and subsequently to an increase of imaging spatial resolving power. The P_{th} value is dependent on the particular compound being investigated, and

can account for the larger spot sizes observed over the biomolecules compared to the polymer photoresist.

It is interesting to note, that previously in laser ablation, laser craters as small as 0.7 μm were observed on high thermal conductivity samples upon 248 nm excimer laser irradiation with a 5.6 μm spot and 25 ns pulse.^[52] The experiments described here, while conducted on low thermal conductivity samples, do show similar behavior and the features smaller than the laser spot size can be resolved. We believe that with a judicious combination of laser spot size and fluence, VUV postionization imaging mass spectrometry will not be limited by diffraction spot size and sub-micron resolution can be achieved. Efforts in this direction are underway. There is however a caveat, as has been shown in the previous discussion on collisional cooling, increasing peak power density leads to enhanced cooling and lower translational energies. However this will lead to larger spot sizes.

A new laser desorption VUV postionization imaging technique and its applicability for imaging of small features on a polymer surface have been demonstrated. This will find application in imaging of a number of biological and geological systems. Recently it has been used to study the effect of antibiotics on bacterial bio-films.^[53] With the methods described here, it is anticipated that chemical composition and change within real-world environmental samples can be visualized with molecular specificity.

To illustrate the capabilities of this method for chemical analysis, representative mass spectra from lignin, cellulose and an extracted soil sample (Suwannee River humic acid) using laser desorption with VUV postionization are shown in Figure 8. This chemical information, when combined with molecular imaging,^[54] will provide valuable new information for studying chemically heterogeneous systems. These systems were chosen to show that tunable VUV coupled with laser desorption is capable of detecting molecular masses between 200-500 Da. While MALDI has been utilized to study many biological systems, there are few techniques that can be applied to small molecules in native environments, as pointed out recently in a review.^[55] Furthermore, previous attempts at laser desorption ionization on similar systems showed extensive pyrolysis type phenomena and fragmentation of molecules.^[56-61] A recent imaging study using MALDI to investigate cellulose in poplar stem has shown that biological matrix effects from lignin and hemicelluloses reduced the sensitivity towards detection of cellulose.^[62]

It is believed that the techniques described here will provide a new way to visualize organic matter with molecular specificity.

Conclusions

Imaging mass spectrometry, utilizing laser desorption of molecules and subsequent synchrotron VUV postionization has been developed at the Chemical Dynamics Beamline at the Advanced Light Source. We characterized this technique by analysis of internal and translational temperatures of laser-desorbed molecules. Two independent techniques show that the internal temperatures of a linear long-chain hydrocarbon and DNA and RNA bases range from 670-800 K. The translational temperatures for DNA and RNA bases are lower and lie in the range of 216-346 K. A dependence of translational temperature on desorption laser power was observed and explained by effective collisional cooling of desorbed molecules. The number of molecules desorbed by a single laser pulse is estimated and compared to the number of molecules expanded during a typical molecular beam experiment under comparable conditions. Estimation of a similar number of molecules under both cases suggests efficient cooling during laser desorption. Initial application of laser desorption imaging mass spectrometry to a polymer pattern on silicon demonstrates its ability to resolve 5 μm features on the sample surface with a 30 μm laser spot size and 7 ns duration.

Experimental Section

The experiment is performed on a secondary ion mass spectrometer (SIMS) coupled to the Chemical Dynamics Beamline (9.0.2) at the Advanced Light Source. The experimental apparatus is essentially the same used recently for the investigation of fragmentation mechanism of lignin monomers coniferyl and sinapyl alcohols.^[63] That apparatus was equipped with a desorption laser allowing synchrotron VUV laser desorption postionization mass spectrometry (VUV-LDPI MS). The laser used for the experiments is a 349 nm Nd:YLF laser, which is triggered externally by the SIMS apparatus master-clock and typically runs at 2500 Hz.

The laser and its focusing optics are mounted directly on the SIMS apparatus so that the laser beam irradiates the sample surface at an angle of 45 degrees. In the experiments described here, the size of the laser spot is approximately 30 μm in diameter. To achieve this spot size, a set of lenses are used. First a diverging lens (focal length $F = -15$ mm) is used to increase the size of beam exiting the laser. The diverging beam is then focused by a set of two converging lenses ($F = 175$ mm and $F = 200$ mm). The distance from the focusing lenses to the sample surface is about 22 cm.

The VUV-LDPI mass spectrometer works as follows: a laser pulse desorbs molecules from the sample surface. The desorbed neutral molecular plume starts to spread perpendicularly from the sample surface; the plume is intersected by a synchrotron VUV beam, which is directed parallel to the sample surface and positioned ~ 20 -50 μm above the surface. The molecules, after being ionized by the VUV light, continue to spread unaffected until application of an extraction electrical field pulse. The extraction pulse is applied 1 to 5 μs after the desorption laser shot. This delay is used to accumulate more ions in the interaction region and eventually obtain mass spectrum with a better signal to noise ratio.

To gather better statistics for the measurements, the sample is rastered and signal for each presented data set was the sum of mass spectra collected from several fresh spots (typically 20-40) on the sample surface. For each surface spot, the data is collected for approximately 10-100 laser shots.

The cellulose, DNA and RNA base samples (all from Sigma Aldrich) used in the current work were prepared by dispersing the chemical compounds in methanol. Only a few drops of the smallest, dispersed particles in the solution were deposited onto a piece of a silicon wafer and air dried. The lignin sample was prepared by placing alkali lignin (Sigma Aldrich) into a beaker

and adding methanol. Methanol did not dissolve all of the lignin, however a few drops of the dissolved solution was deposited onto the silicon wafer and air dried. The humic acid sample (International Humic Substances Society) was prepared by directly placing < 1 mg of powder onto a silicon substrate. Several drops of methanol were applied on top of the powder to dissolve and disperse the humic acids before being allowed to air dry.

For determination of translational energies, the sample was placed 800 μm below the VUV beam. To determine the distance precisely, a measurement of synchrotron light profile was performed. A sample stage coordinate Z (height) was scanned and the electric current on the sample produced by impinging VUV radiation was measured. Differentiation of the sample's current as a function of Z-coordinate generated a Gaussian-like light profile with a maximum corresponding to the center of VUV beam. The stage was lowered by 800 μm relative to this coordinate. The extraction potential was changed correspondingly to maintain the extraction field such that photoionized neutrals would experience a 2000 V potential difference from the point of ionization to the extractor cone.

In contrast to measurements of regular mass spectra, where a short extraction pulse of 2-5 μs duration is applied with a delay of 1-5 μs after the desorption laser shot, translational energy TOF distributions were measured using long, 50 μs extraction pulses that were applied simultaneously with the desorption laser shot. Therefore the motion of desorbed molecules occurs in the presence of an extraction field. Under the desorption conditions used, no molecular prompt ions were detected. Therefore, the initial motion of the molecules is unaffected by the presence of the extraction field. When the fast molecules reach the quasi-continuous synchrotron VUV beam, they are ionized and immediately extracted into the TOF-MS. Hence, due to the continuous VUV light, the distribution of molecules as a function of time for a single laser shot can be measured. Typical TOF distributions for DNA and RNA bases are shown in Figure 4.

Acknowledgements

The authors (O.K.) thank Terefe Habteyes (UC Berkeley) and Xianglei Mao (LBNL) for help with atomic force microscopy and optical surface profilometry of the adenine sample, and Deirdre Olynick (LBNL) for providing the polymer sample for testing of imaging capabilities. This work is supported by the Director, Office of Energy Research, Office of Basic Energy Sciences,

Chemical Sciences Division of the U.S. Department of Energy under contract No. DE-AC02-05CH11231.

Citations

- [1] P. K. Quinn, T. S. Bates, D. J. Coffman, D. S. Covert *Atmos. Chem. Phys.* **2008**, 8, 1029-1042.
- [2] D. G. Castner, B. D. Ratner *Surf. Sci.* **2002**, 500, 28-60.
- [3] S. G. Ostrowski, C. T. Van Bell, N. Winograd, A. G. Ewing *Science*. **2004**, 305, 71-73.
- [4] M. E. Himmel, S. Y. Ding, D. K. Johnson, W. S. Adney, M. R. Nimlos, J. W. Brady, T. D. Foust *Science*. **2007**, 315, 804-807.
- [5] R. Singh, D. Paul, R. K. Jain *Trends Microbiol.* **2006**, 14, 389-397.
- [6] P. Metzger, C. Largeau *Appl. Microbiol. Biotechnol.* **2005**, 66, 486-496.
- [7] I. A. Guschina, J. L. Harwood *Prog. Lipid Res.* **2006**, 45, 160-186.
- [8] Q. Chen, D. K. Farmer, J. Schneider, S. R. Zorn, C. L. Heald, T. G. Karl, A. Guenther, J. D. Allan, N. Robinson, H. Coe, J. R. Kimmel, T. Pauliquevis, S. Borrmann, U. Poschl, M. O. Andreae, P. Artaxo, J. L. Jimenez, S. T. Martin *Geophys. Res. Lett.* **2009**, 36, 5.
- [9] J. De Gouw, J. L. Jimenez *Environ. Sci. Technol.* **2009**, 43, 7614-7618.
- [10] E. R. Graber, Y. Rudich *Atmos. Chem. Phys.* **2006**, 6, 729-753.
- [11] R. Sutton, G. Sposito *Environ. Sci. Tech.* **2005**, 39, 9009-9015.
- [12] M. Kleber *Environ. Chem.* **2010**, 7, 320-332.
- [13] K. R. Wilson, M. Jimenez-Cruz, C. Nicolas, L. Belau, S. R. Leone, M. Ahmed *J. Phys. Chem. A.* **2006**, 110, 2106-2113.
- [14] J. Zhou, L. K. Takahashi, K. R. Wilson, S. R. Leone, M. Ahmed *Anal. Chem.* **2010**, 82, 3905-3913.
- [15] E. Gloaguen, E. R. Mysak, S. R. Leone, M. Ahmed, K. R. Wilson *Int. J. Mass Spectrom.* **2006**, 258, 74-85.
- [16] L. Hanley, R. Zimmermann *Anal. Chem.* **2009**, 81, 4174-4182.
- [17] E. Nir, H. E. Hunziker, M. S. de Vries *Anal. Chem.* **1999**, 71, 1674-1678.
- [18] R. J. Levis *Annu. Rev. Phys. Chem.* **1994**, 45, 483-518.
- [19] L. Hanley, O. Kornienko, E. T. Ada, E. Fuoco, J. L. Trevor *J. Mass Spectrom.* **1999**, 34, 705-723.
- [20] R. Knochenmuss *Analyst.* **2006**, 131, 966-986.
- [21] R. Knochenmuss, L. V. Zhigilei *J. Mass Spectrom.* **2010**, 45, 333-346.
- [22] B. J. Garrison, Z. Postawa *Mass Spectrom. Rev.* **2008**, 27, 289-315.
- [23] E. Woods, R. E. Miller, T. Baer *J. Phys. Chem. A.* **2003**, 107, 2119-2125.
- [24] B. Oktem, M. P. Tolocka, M. V. Johnston *Anal. Chem.* **2004**, 76, 253-261.
- [25] R. C. Shea, C. J. Petzold, J. A. Liu, H. I. Kenttamaa *Anal. Chem.* **2007**, 79, 1825-1832.
- [26] C. D. Mowry, M. V. Johnston *J. Phys. Chem.* **1994**, 98, 1904-1909.
- [27] M. J. Frisch, G. W. Trucks, H. B. Schlegel, G. E. Scuseria, M. A. Robb, J. R. Cheeseman, J. A. Montgomery Jr., T. Vreven, K. N. Kudin, J. C. Burant, J. M. Millam, S. S. Iyengar, J. Tomasi, V. Barone, B. Mennucci, M. Cossi, G. Scalmani, N. Rega, G. A. Petersson, H. Nakatsuji, M. Hada, M. Ehara, K. Toyota, R. Fukuda, J. Hasegawa, M. Ishida, T. Nakajima, Y. Honda, O. Kitao, H. Nakai, M. Klene, X. Li, J. E. Knox, H. P. Hratchian, J. B. Cross, C. Adamo, J. Jaramillo, R. Gomperts, R. E. Stratmann, O. Yazyev, A. J. Austin, R. Cammi, C. Pomelli, J. W. Ochterski, P. Y. Ayala, K. Morokuma, G. A. Voth, P. Salvador, J. J. Dannenberg, V. G. Zakrzewski, S. Dapprich, A. D. Daniels, M. C. Strain, O. Farkas, D. K. Malick, A. D. Rabuck, K. Raghavachari, J. B. Foresman, J. V. Ortiz, Q. Cui, A. G. Baboul, S. Clifford, J. Cioslowski, B. B. Stefanov, G. Liu, A. Liashenko, P. Piskorz, I. Komaromi, R. L. Martin, D. J. Fox, T. Keith, M. A. Al-Laham, C. Y. Peng, A. Nanayakkara, M. Challacombe, P. M. W. Gill, B. Johnson, W. Chen, M. W. Wong, C. Gonzalez, J. A. Pople in *Gaussian 03*, Gaussian, Inc., Wallingford, CT, **2004**.

- [28] K. B. Bravaya, O. Kostko, M. Ahmed, A. I. Krylov *Phys. Chem. Chem. Phys.* **2010**, 12, 2292-2307.
- [29] O. Kostko, K. Bravaya, A. Krylov, M. Ahmed *Phys. Chem. Chem. Phys.* **2010**, 12, 2860-2872.
- [30] A. Amirav, U. Even, J. Jortner *Chem. Phys.* **1980**, 51, 31-42.
- [31] K. B. Bravaya, O. Kostko, S. Dolgikh, A. Landau, M. Ahmed, A. I. Krylov *J. Phys. Chem. A.* **2010**, 114, 12305-12317.
- [32] K. W. Choi, J. H. Lee, S. K. Kim *J. Am. Chem. Soc.* **2005**, 127, 15674-15675.
- [33] V. M. Orlov, A. N. Smirnov, Y. M. Varshavsky *Tetrahedron Lett.* **1976**, 4377-4378.
- [34] H. W. Jochims, M. Schwell, H. Baumgartel, S. Leach *Chem. Phys.* **2005**, 314, 263-282.
- [35] W. Genuit, N. M. M. Nibbering *Int. J. Mass Spectrom. Ion Process.* **1986**, 73, 61-80.
- [36] M. L. Vestal *J. Chem. Phys.* **1965**, 43, 1356-&.
- [37] B. Steiner, C. F. Giese, M. G. Inghram *J. Chem. Phys.* **1961**, 34, 189-&.
- [38] B. Spengler, U. Bahr, M. Karas, F. Hillenkamp *Anal. Instrum.* **1988**, 17, 173-193.
- [39] S. T. Tsai, C. H. Chen, Y. T. Lee, Y. S. Wang *Mol. Phys.* **2008**, 106, 239-247.
- [40] J. W. Elam, D. H. Levy *J. Phys. Chem. B.* **1998**, 102, 8113-8120.
- [41] F. Engelke, J. H. Hahn, W. Henke, R. N. Zare *Anal. Chem.* **1987**, 59, 909-912.
- [42] T. Huthfahre, C. H. Becker *Rapid Commun. Mass Spectrom.* **1991**, 5, 378-382.
- [43] D. H. Levy *Science.* **1981**, 214, 263-269.
- [44] S. Y. T. Van De Meerakker, H. L. Bethlem, G. Meijer *Nat. Phys.* **2008**, 4, 595-602.
- [45] A. A. Puretzky, D. B. Geohegan *Chem. Phys. Lett.* **1998**, 286, 425-432.
- [46] D. R. Ermer, M. Baltz-Knorr, R. F. Haglund *J. Mass Spectrom.* **2001**, 36, 538-545.
- [47] D. J. Krajnovich *J. Chem. Phys.* **1995**, 102, 726-743.
- [48] S. Georgiou, A. Koubenakis, J. Labrakis, M. Lassithiotaki *Appl. Surf. Sci.* **1998**, 127, 122-127.
- [49] C. Grivas, H. Niino, A. Yabe *Appl. Phys. A-Mater. Sci. Process.* **1999**, 69, S159-S163.
- [50] J. M. Liu *Opt. Lett.* **1982**, 7, 196-198.
- [51] S. Martin, A. Hertwig, M. Lenzner, J. Kruger, W. Kautek *Appl. Phys. A-Mater. Sci. Process.* **2003**, 77, 883-884.
- [52] I. Avrutsky, D. G. Georgiev, D. Frankstein, G. Auner, G. Newaz *Appl. Phys. Lett.* **2004**, 84, 2391-2393.
- [53] G. L. Gasper, L. K. Takahashi, J. Zhou, M. Ahmed, J. F. Moore, L. Hanley *Anal. Chem.* **2010**, 82, 7472-7478.
- [54] R. Y. Tsien *Nat. Rev. Mol. Cell Biol.* **2003**, SS16-SS21.
- [55] A. Svatos *Trends Biotechnol.* **2010**, 28, 425-434.
- [56] S. M. Mugo, C. S. Bottaro *Rapid Commun. Mass Sp.* **2004**, 18, 2375-2382.
- [57] T. Ferge, F. Muhlberger, R. Zimmermann *Anal. Chem.* **2005**, 77, 4528-4538.
- [58] V. Samburova, R. Zenobi, M. Kalberer *Atmos. Chem. Phys.* **2005**, 5, 2163-2170.
- [59] Z. Li, L. Q. Chu, J. V. Sweedler, P. W. Bohn *Anal. Chem.* **2010**, 82, 2608-2611.
- [60] S. Reale, A. Di Tullio, N. Spreti, F. De Angelis *Mass Spectrom. Rev.* **2004**, 23, 87-126.
- [61] E. M. Pena-Mendez, D. Gajdosova, K. Novotna, P. Prosek, J. Havel *Talanta.* **2005**, 67, 880-890.
- [62] S. Jung, Y. F. Chen, M. C. Sullards, A. J. Ragauskas *Rapid Commun. Mass Sp.* **2010**, 24, 3230-3236.
- [63] L. K. Takahashi, J. Zhou, O. Kostko, A. Golan, S. R. Leone, M. Ahmed *J. Phys. Chem. A.* **2011**, 115, 3279-3290.

Table 1. Mean and most probable translational velocities and translational energies for biomolecules studied in this work.

molecule	T_{tr} [K] ^[a]	m/z	v_{mean} [m/s] ^[b]	v_{prob} [m/s] ^[c]	E_{tr} [eV] ^[d]
adenine	216	135	184	163	0.019
thymine	329	126	235	208	0.028
cytosine	346	111	257	228	0.030
uracil	298	112	237	210	0.026

[a] Translational temperature, [b] mean translational velocity, [c] the most probable translational velocity, [d] translational energy.

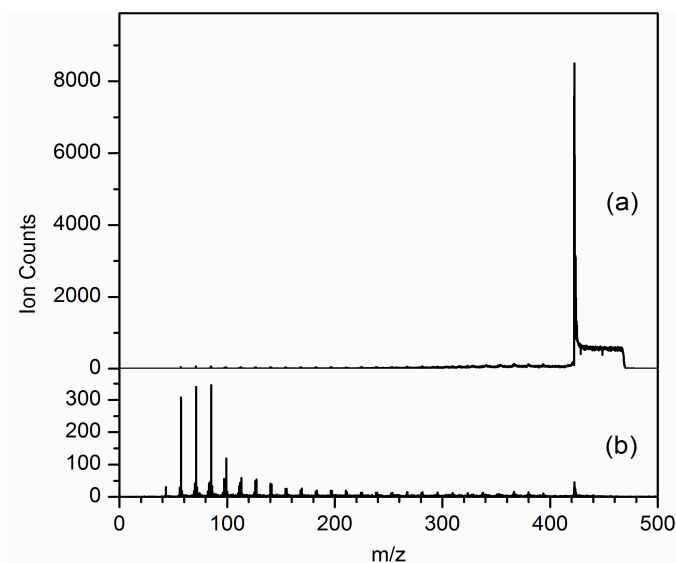


Figure 1. 10.5 eV photoionization mass spectra of triacontane at various experimental conditions: (a) thermally evaporated at 373 K and (b) laser desorbed.

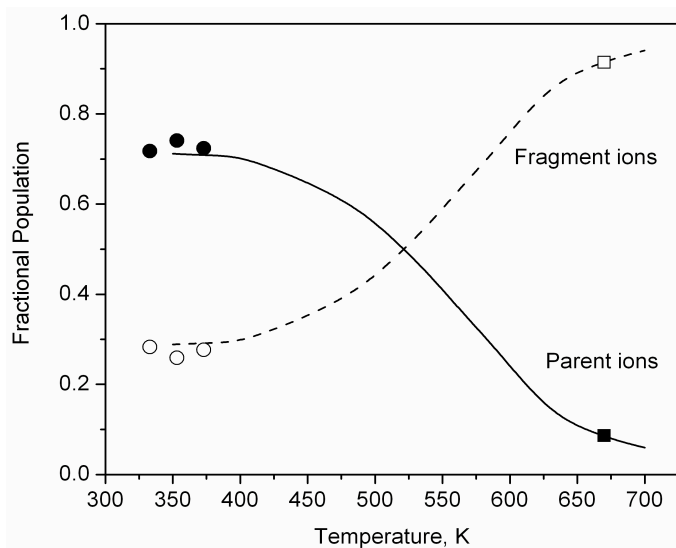


Figure 2. Temperature dependent fractional populations of triacontane parent ions (solid line) and fragment ions (dashed line). Open and filled circles correspond to fractional population obtained using a heating/cooling stage. The fractional population corresponding to laser desorbed triacontane is shown by squares: fragment ions are indicated by the black open square and parent ions by the black filled square.

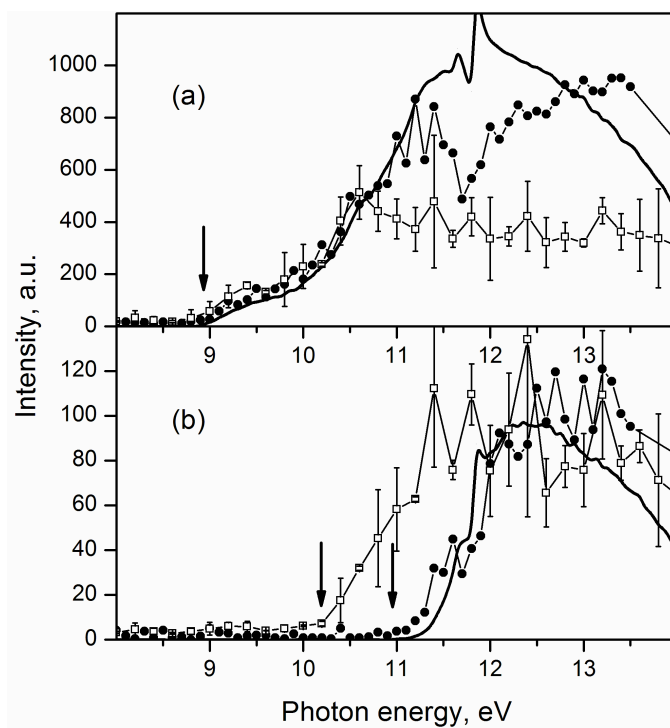


Figure 3. Photoionization efficiency curves for (a) thymine parent and (b) its fragment $m/z=83$. Solid black lines correspond to the molecular beam experiment, filled black circles correspond to thermal evaporation at 313 K and open black squares correspond to the laser desorption postionization experiment. The arrows indicate ionization or appearance energies.

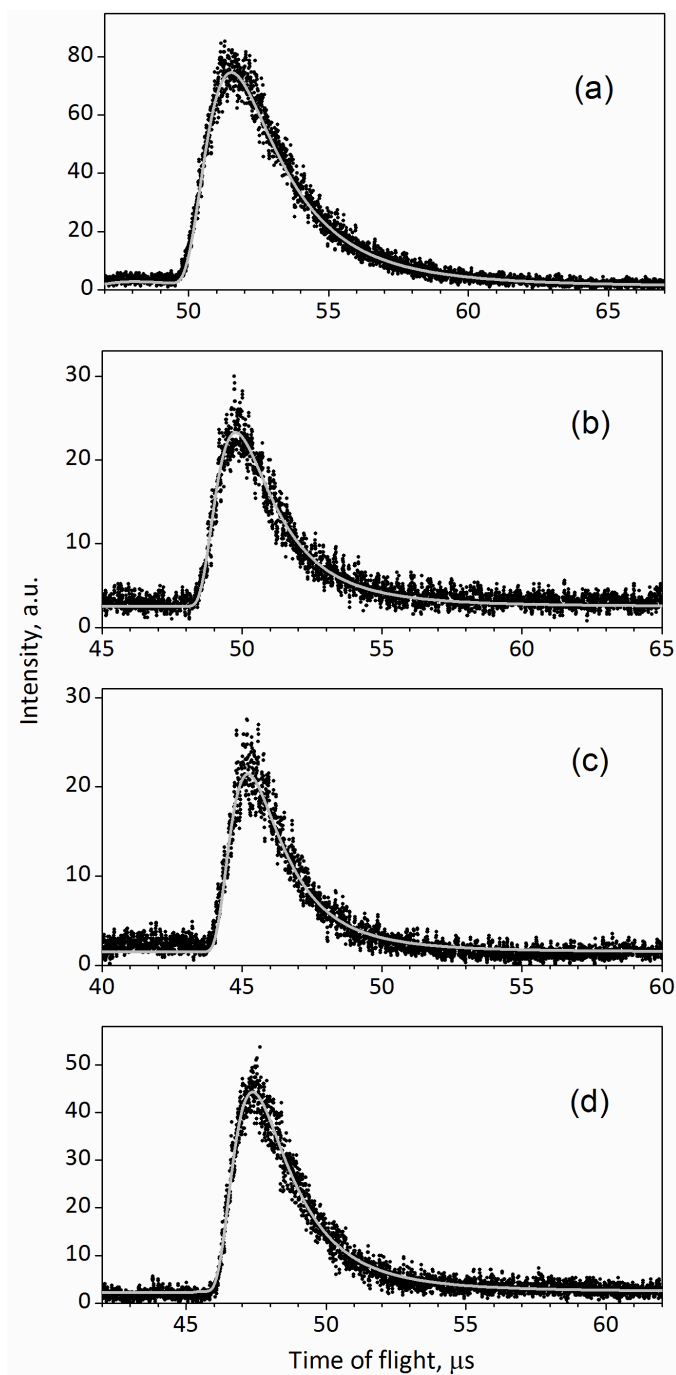


Figure 4. Time of flight spectra for: (a) adenine, (b) thymine, (c) cytosine, and (d) uracil. The spectra are shown together with half-space Maxwell-Boltzmann fit curves.

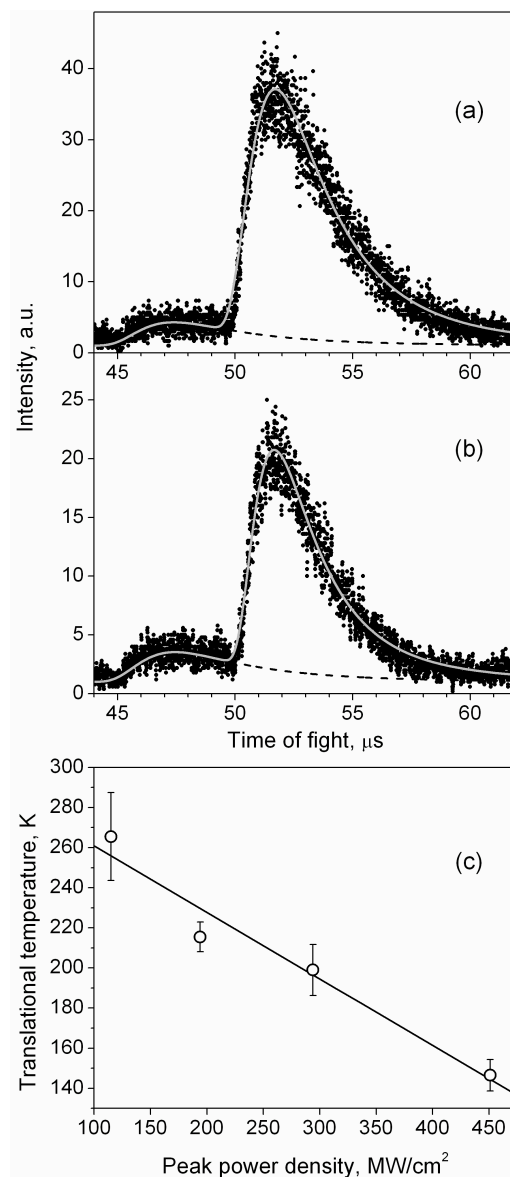


Figure 5. TOF spectra for adenine, desorbed under various conditions: desorption laser peak power density of (a) 451 MW/cm^2 and (b) 194 MW/cm^2 . The grey lines represent the fit of the experimental data with the Maxwell-Boltzmann distribution. The dashed lines correspond to the fit of adenine fragment $m/z=119$, and the main features peaking around 51.5 μs correspond to the adenine ($m/z=135$) signal. Translational temperatures of the adenine molecules, obtained from the fit of experimental TOF distributions for different laser peak power densities, are shown in panel (c). The solid line in panel (c) corresponds to the linear fit of the data and is shown to guide the eye.

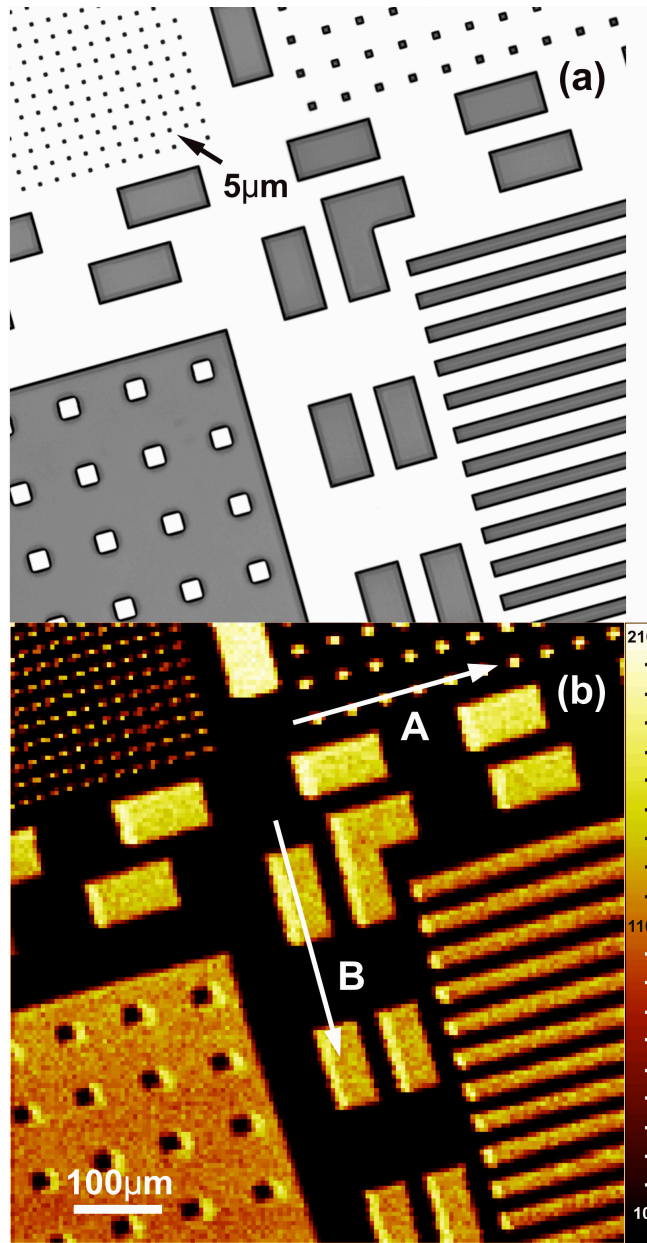


Figure 6. (a) Optical microscope and (b) laser desorption positionization images of photoresist features on a silicon wafer. In the optical image the dark features correspond to photoresist and white to silicon substrate. In (b) the color corresponds to intensity of $m/z=165$ signal (the brighter the signal, the higher the intensity). A and B shows positions of signal profiles shown in Figure 7 (b, c).

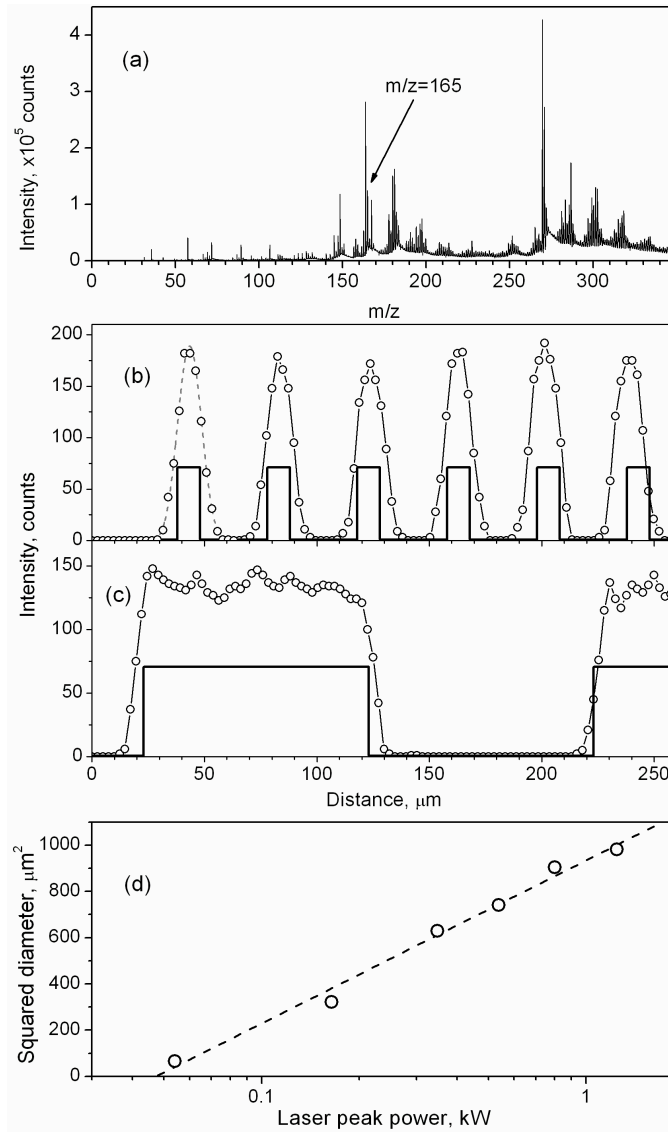


Figure 7. (a) Mass spectrum of a photoresist, covering the sample used for imaging. (b) and (c) $m/z=165$ signal profiles, corresponding to section A and B in Figure 7(b), correspondingly. Solid lines in (b) and (c) are idealized feature profiles. Gray dashed line in (b) corresponds to the fit to the experimental data accounting for the Gaussian profile of the laser intensity. (d) Squared diameter of the desorbed area in dependence on the laser peak power. Dashed line in (d) corresponds to fit of the experimental data with eq. (5).

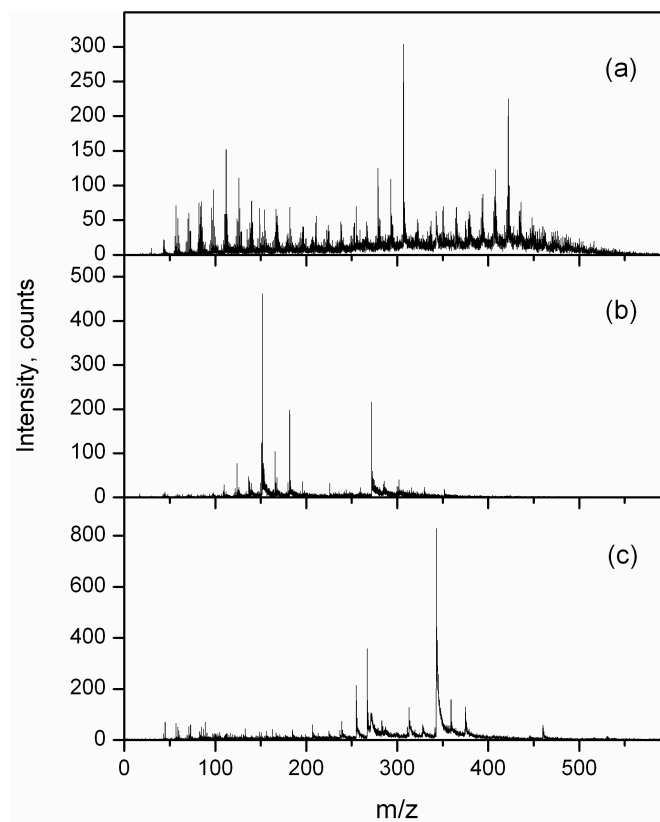
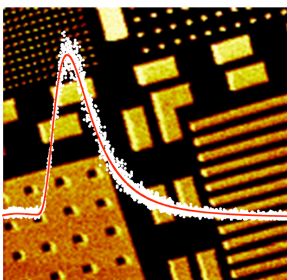


Figure 8. 10.5 eV photoionization mass spectra for laser desorbed (a) Suwannee River humic acid, (b) lignin, and (c) cellulose.

Graphical Abstract for the Table of Content



Don't blow me up: An imaging mass spectroscopy technique using laser desorption and VUV postionization has been characterized. It promises good spatial resolution and leads to minimal molecular fragmentation.

This document was prepared as an account of work sponsored by the United States Government. While this document is believed to contain correct information, neither the United States Government nor any agency thereof, nor the Regents of the University of California, nor any of their employees, makes any warranty, express or implied, or assumes any legal responsibility for the accuracy, completeness, or usefulness of any information, apparatus, product, or process disclosed, or represents that its use would not infringe privately owned rights. Reference herein to any specific commercial product, process, or service by its trade name, trademark, manufacturer, or otherwise, does not necessarily constitute or imply its endorsement, recommendation, or favoring by the United States Government or any agency thereof, or the Regents of the University of California. The views and opinions of authors expressed herein do not necessarily state or reflect those of the United States Government or any agency thereof or the Regents of the University of California.